Title

Hippo signaling pathway activation during SARS-CoV-2 infection contributes to host antiviral response

Journal

PLOS Biology, 20(11)

ISSN

1544-9173

Authors

Garcia, Gustavo
Jeyachandran, Arjit Vijey
Wang, Yijie
et al.

Publication Date

2022

DOI

10.1371/journal.pbio.3001851

Peer reviewed

PLOS BIOLOGY

RESEARCH ARTICLE

Hippo signaling pathway activation during SARS-CoV-2 infection contributes to host antiviral response

Gustavo Garcia, Jr.[1], Arjit Vijey Jeyachandran[1], Yijie Wang[2], Joseph Ignatius Irudayam[1], Sebastian Castillo Cario[1], Chandani Sen[3], Shen Li[2], Yunfeng Li[4], Ashok Kumar[5], Karin Nielsen-Saines[3], Samuel W. French[6], Priya S. Shah[7], Kouki Morizono[8,9], Brigitte N. Gomperts[3,6,10,11], Arjun Deb[2,10,11,12,13], Arunachalam Ramaiah[14,15,16]*, Vaithilingaraja Arumugaswami[1,10,12]*

1 Department of Molecular and Medical Pharmacology, University of California, Los Angeles, California, United States of America, **2** Division of Cardiology, Department of Medicine, David Geffen School of Medicine, UCLA, Los Angeles, California, United States of America, **3** UCLA Children's Discovery and Innovation Institute, Mattel Children's Hospital UCLA, Department of Pediatrics, David Geffen School of Medicine, UCLA, Los Angeles, California, United States of America, **4** Translational Pathology Core Laboratory, Department of Pathology and Laboratory Medicine, David Geffen School of Medicine, UCLA, Los Angeles, California, United States of America, **5** Department of Ophthalmology, Visual and Anatomical Sciences, Wayne State University, Detroit, Michigan, United States of America, **6** Jonsson Comprehensive Cancer Center, UCLA, Los Angeles, California, United States of America, **7** Department of Chemical Engineering, University of California, Davis, California, United States of America, **8** Division of Hematology and Oncology, Department of Medicine, David Geffen School of Medicine, University of California, Los Angeles, California, United States of America, **9** UCLA AIDS Institute, David Geffen School of Medicine, University of California, Los Angeles, California, United States of America, **10** Eli & Edythe Broad Center of Regenerative Medicine and Stem Cell Research, UCLA, Los Angeles, California, United States of America, **11** Molecular Biology Institute, UCLA, Los Angeles, California, United States of America, **12** California Nanosystems Institute, UCLA, Los Angeles, California, United States of America, **13** Department of Molecular, Cell and Developmental Biology, Division of Life Sciences, University of California, Los Angeles, California, United States of America, **14** Tata Institute for Genetics and Society, Centre at inStem, Bangalore, India, **15** Department of Ecology and Evolutionary Biology, University of California, Irvine, California, United States of America, **16** Section of Cell and Developmental Biology, University of California, San Diego, California, United States of America

* arunachalam@tigs.res.in (AR); varumugaswami@mednet.ucla.edu (VA)

Citation: Garcia G, Jr., Jeyachandran AV, Wang Y, Irudayam JI, Cario SC, Sen C, et al. (2022) Hippo signaling pathway activation during SARS-CoV-2 infection contributes to host antiviral response. PLoS Biol 20(11): e3001851. https://doi.org/10.1371/journal.pbio.3001851

Academic Editor: Eng Eong Ooi, Duke-NUS: Duke-NUS Medical School, SINGAPORE

Received: January 13, 2022

Accepted: September 26, 2022

Published: November 8, 2022

Data Availability Statement: The gene expression data used in this study were retrieved at Gene Expression Omnibus with accession numbers GSE150316 and GSE150392. All data used and referred to in the manuscript using the following format verbatim: S1 Data, S2 Data, etc. can be found in the 'Supporting Information' file.

Funding: This work was supported by University of California, Los Angeles (UCLA) David Geffen School of Medicine (DGSOM); The Broad Stem Cell Research Center (OCRC #20-15 to VA); UCLA W.

Abstract

Severe Acute Respiratory Syndrome Coronavirus 2 (SARS-CoV-2), responsible for the Coronavirus Disease 2019 (COVID-19) pandemic, causes respiratory failure and damage to multiple organ systems. The emergence of viral variants poses a risk of vaccine failures and prolongation of the pandemic. However, our understanding of the molecular basis of SARS-CoV-2 infection and subsequent COVID-19 pathophysiology is limited. In this study, we have uncovered a critical role for the evolutionarily conserved Hippo signaling pathway in COVID-19 pathogenesis. Given the complexity of COVID-19-associated cell injury and immunopathogenesis processes, we investigated Hippo pathway dynamics in SARS-CoV-2 infection by utilizing COVID-19 lung samples and human cell models based on pluripotent stem cell-derived cardiomyocytes (PSC-CMs) and human primary lung air–liquid interface (ALI) cultures. SARS-CoV-2 infection caused activation of the Hippo signaling pathway in COVID-19 lung and in vitro cultures. Both parental and Delta variant of concern (VOC) strains induced Hippo pathway. The chemical inhibition and gene knockdown of upstream

M. Keck Foundation COVID-19 Research Award to VA; National Institute of Health (1R01EY032149-01 and 5R01AI163216-02 to VA; 1R01DK132735-01 to VA and AD; 1R01CA208303 to BG); The National Institute of Health (R01AI145044 to KM; U19AI149504 to KM); The Tata Institute for Genetics and Society, India to AR. The funders had no role in study design, data collection and analysis, decision to publish, or preparation of the manuscript.

Competing interests: The authors have declared that no competing interests exist.

Abbreviations: ABSC, airway basal stem cell; ACE2, angiotensin-converting enzyme 2; ALI, air–liquid interface; AMD, age-related macular degeneration; ARDS, acute respiratory distress syndrome; CNV, choroidal neovascularization; CPE, cytopathic effect; COVID-19, Coronavirus Disease 2019; DDR, DNA-damage response; DEG, differentially expressed gene; FBS, fetal bovine serum; FDR, false discovery rate; hPSC-CM, human pluripotent stem cell-derived cardiomyocyte; GEO, Gene Expression Omnibus; KEGG, Kyoto Encyclopedia of Genes and Genomes; MOI, multiplicity of infection; NIAID, National Institute of Allergy and Infectious Diseases; PSC-CM, pluripotent stem cell-derived cardiomyocyte; SARS-CoV-2, Severe Acute Respiratory Syndrome Coronavirus 2; TAC, transverse aortic constriction; VOC, variant of concern; ZIKV, Zika virus.

kinases MST1/2 and LATS1 resulted in significantly enhanced SARS-CoV-2 replication, indicating antiviral roles. Verteporfin, a pharmacological inhibitor of the Hippo pathway downstream transactivator, YAP, significantly reduced virus replication. These results delineate a direct antiviral role for Hippo signaling in SARS-CoV-2 infection and the potential for this pathway to be pharmacologically targeted to treat COVID-19.

Introduction

Severe Acute Respiratory Syndrome-related Coronavirus 2 (SARS-CoV-2) is a betacoronavirus of zoonotic origin having similarity with bat SARS-CoV-like viruses. SARS-CoV-2 is responsible for the outbreak of the Coronavirus Disease 2019 (COVID-19) pandemic leading to over 5 million deaths and 270 million cases worldwide [1–3]. SARS-CoV-2 primarily causes severe lung injury with diffuse alveolar damage resulting in the development of acute respiratory distress syndrome (ARDS) [4]. The virus is also known to infect heart, kidney, brain, and digestive systems due to the widespread expression of host cell surface membrane receptor angiotensin-converting enzyme 2 (ACE2) and other receptors, including NRP1, AXL, and CD147 [5–11]. Therefore, patients develop additional systemic complications including acute kidney injury [12–14], vascular inflammation (endotheliitis), and cardiac complications, including circulatory collapse and pathologic arrhythmias [15,16]. Viral replication-mediated epithelial cell injuries result in a vigorous immune response leading to organ failure, and possibly death in severe cases. Patients with various underlying conditions such as cardiovascular diseases, diabetes, and obesity are linked with increased risk of COVID-19 mortality [17,18].

To replicate, viruses hijack cellular machinery and signaling pathways. Thus, understanding the molecular basis of dysregulated signaling circuitry can provide potential therapeutic targets. Utilizing a library of kinase inhibitors, we previously demonstrated critical pathways that are important for SARS-CoV-2 virus replication such as the DNA-damage response (DDR), mTOR-PI3K-AKT, and ABL-BCR/MAPK pathways [19]. COVID-19 pathogenesis is a complex process involving crosstalk with multiple cellular pathways. To understand the fundamental principles underlying RNA viral mediated cell injury processes, we hypothesize that the conserved cellular circuitry of the Hippo signaling pathway, which is involved in tissue growth, immune response, and inflammation, can contribute to regulating SARS-CoV-2 replication and COVID-19 pathogenesis. Previously, we observed that the Zika virus (ZIKV), a member of the *Flaviviridae* family, activates this pathway [20]. The core components of the Hippo pathway in mammals are STE20-like kinases STK4/MST1 and STK3/MST2 (Hpo in *Drosophila*), large tumor suppressors (LATS1/2, Wts in *Drosophila*), MOB kinase activator 1A and 1B (Mats in *Drosophila*), Neurofibromatosis 2 (NF2), and Salvador 1 (SAV1) [21]. MST1/2 and LATS1/2 are serine/threonine kinases, whereas NF2 and SAV1 are adaptors or co-factors. Upon activation by stimuli, MST1/2 phosphorylate and activates the downstream serine/threonine kinase LATS1/2. LATS1/2 can be phosphorylated by MAP4Ks independent of MST1/2 axis. The phospho-LATS1/2, along with SAV1, then phosphorylates YAP (Yes-associated protein), a transcription co-activator and oncogene. Phospho-YAP, bound to a 14-3-3 protein and retained in the cytoplasm, is subsequently ubiquitinated and degraded by proteasomes. While the Hippo pathway is inactive, the unphosphorylated YAP and its homologous partner TAZ translocate to the nucleus, where they bind to the TEAD family of transcription factors and mediate expression of target genes involved in cell survival and proliferation (Birc5, Id, CTCF, Axin2, Myc, CycD, etc.) [22]. As the Hippo signaling pathway controls progenitor cell

proliferation and differentiation, and the size of organs [23–27], the pathway is closely linked to mitochondrial energy metabolism and biogenesis. Studies suggest that the Hippo pathway modulates host antiviral immune responses [28–33], where YAP inhibits antiviral defense mechanisms by antagonizing the function of pro-innate immune factor TBK1 [34], which is a key signal transducer of cytosolic RNA-sensing retinoic acid-inducible gene I (RIG-I)-like receptor (RLR) pathway. Inherited autosomal recessive mutations of MST1 (STK4) in human have been attributed to primary immunodeficiency with T- and B cell lymphopenia, neutropenia, and defective regulatory T cells [30,35–37]. Thus, we postulate that Hippo signaling pathway plays a critical role in SARS-CoV-2 antiviral response and COVID-19 pathogenesis.

Results/Discussion

To understand the pathophysiological effect of SARS-CoV-2 on the Hippo signaling pathway, first we performed transcriptomic analysis of previously published RNA sequencing (RNA-seq) datasets of lung samples from COVID-19 patients ($n = 5$) [38]. The Kyoto Encyclopedia of Genes and Genomes (KEGG) pathway analysis indicates that many genes (45 genes) in the Hippo pathway were differentially regulated ($p < 0.01$ and log2FC>1) (Fig 1A and S1 Data), and 33 (73%) of these genes are up-regulated, likely due to an antiviral host response. WWTR1/TAZ, a YAP homologue and downstream transcriptional coactivator of the Hippo signaling pathway, was found to be significantly down-regulated, suggesting the activation of Hippo signaling pathway. Phosphorylation of YAP (phospho-YAP) at Serine (Ser or S) 127 is a hallmark of Hippo pathway activation and results in cytoplasmic retention and inactivation of its transactivation function. We investigated YAP/TAZ phosphorylation status by immunohistochemical staining and analysis of 4 autopsy lung tissue samples from COVID-19 patients and control lungs (Fig 1B). Three of the samples were positive for the phospho-YAP (Ser127) phenotype. Using RNA-fluorescence in situ hybridization (RNA-FISH), SARS-CoV-2 viral genomes were detected in the COVID-19 lung tissue (Fig 1B). In addition, immunohistochemistry demonstrated a higher level of phospho-YAP (Ser127) in the COVID-19 lung compared to control lung (Fig 1B). Furthermore, we observed that the COVID-19 lung had heavy infiltration of CD68-positive (+) mononuclear inflammatory cells (S1A Fig). CD68 marks macrophages in the inflammatory milieu. The influx of CD68+ cells in the COVID-19 lung could be due to tissue damage caused by virus replication. The Hippo pathway activation in COVID-19 lung can induce Type I IFN signaling pathway that can contribute to host antiviral inflammatory response.

The host response to virus infection is a dynamic process. The temporal differences in the time of virus infection and the progression to severe disease in COVID-19 patients can contribute to the expression and phosphorylation levels of YAP. Thus, to investigate SARS-CoV-2 viral replication and the Hippo signaling pathway in a well-controlled experimental system, we utilized a biologically relevant primary human proximal airway cell culture model, which consisted of mucociliary epithelial cells grown at an air–liquid interface (ALI). Human lung airway basal stem cells (ABSC) harvested from the trachea and bronchi of healthy lungs were differentiated into a ciliated pseudostratified columnar epithelium in a collagen-coated transwell membrane culture system [19,39,40]. The ciliated and secretory airway epithelial cell types in the ALI culture were verified using immunostaining for the cell type-specific markers, acetylated tubulin and Mucin5AC, respectively (Fig 1C). The apical surface of the ALI cultures was exposed to SARS-CoV-2 infection to understand how the virus affects the Hippo pathway at a post-translational level. Parental SARS-CoV-2 (Isolate USA-WA1/2020 at MOI of 1) from BEI Resources was used for infection studies in the UCLA BSL3 high-containment facility. In all in vitro experiments, we used 48 hours post-infection as a common endpoint. Since primary ALI

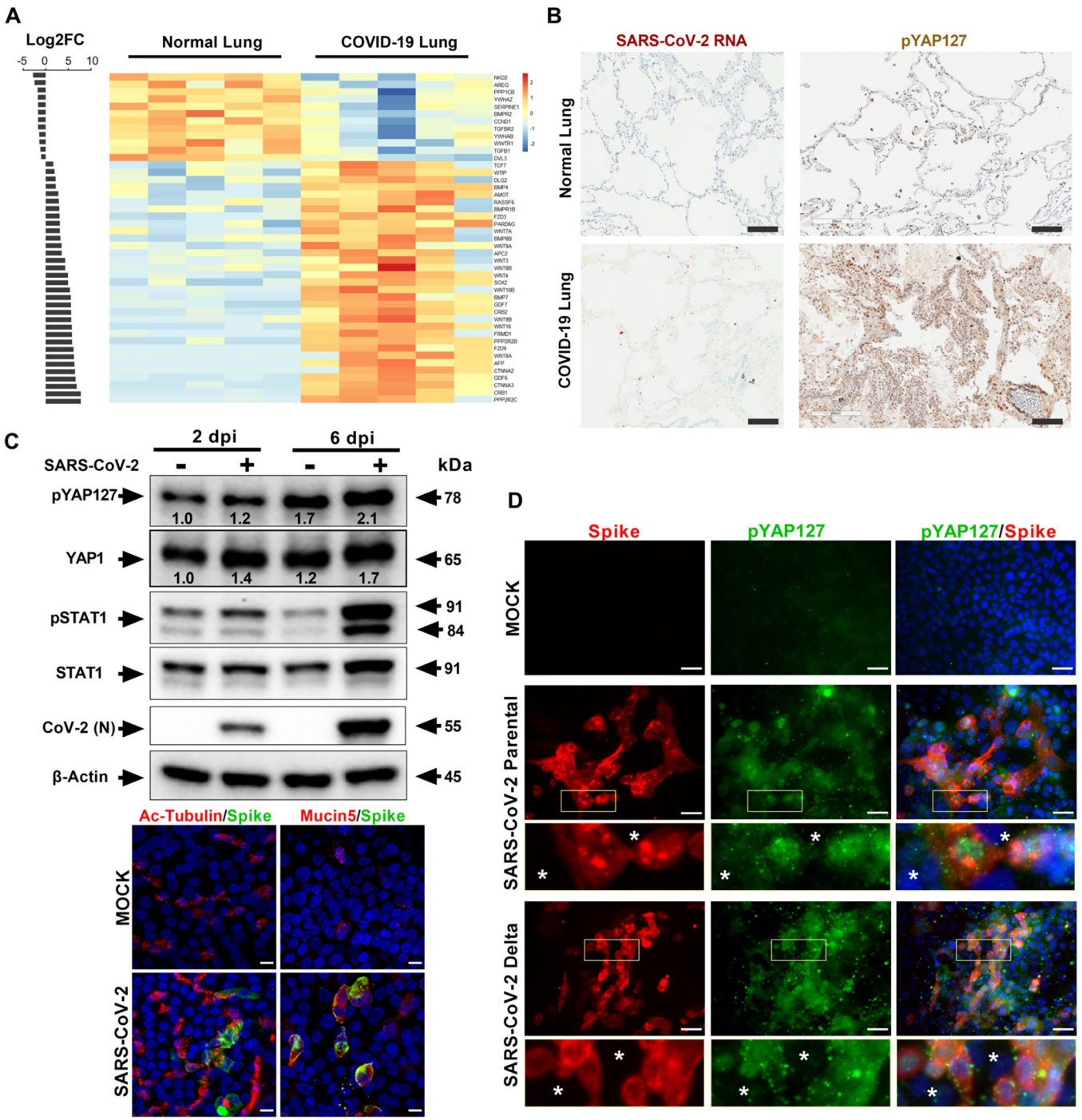

Fig 1. Hippo signaling pathway is activated in lung tissues of COVID-19 and infected human lung in vitro cell cultures. (A) Transcriptome analysis of normal and COVID-19 autopsy lung samples ($n = 5$) is presented. Bar graph shows Log2FC (FC >1) of 45 Hippo signaling pathway genes that were differentially expressed in COVID-19 lung samples ($p < 0.01$). The adjacent heatmap depicts Z scores as expression levels of these 45 DEGs. Blue and red colors represent 12 down-regulated and 33 up-regulated genes, respectively. The KEGG pathway database was used to examine the Hippo signaling pathway genes in the differentially expressed gene list. Individual quantitative observations that underlie the data summarized can be located under the Supporting Information File as S1 Data. (B) IHC of COVID-19 lung autopsy tissue shows high level of phospho-YAP Ser127 protein (dark brown). SARS-CoV-2 RNA (red) presence in COVID-19 lung was confirmed by RNA-FISH (RNAscope) (scale bar: 100 μm). (C) Western blot analyses of lung ALI cells show activation of Hippo-STAT1 pathways during SARS-CoV-2 infection (MOI 1). Density of bands compared to that of 2 dpi mock is provided for pYAP127 and YAP. Proximal lung air interface cultures are susceptible to SARS-CoV-2 infection. Antibody targeting Spike protein (green) was used for probing infection by immunohistochemistry. Cell-specific markers, such as Ac-tubulin (ciliated cells) and Mucin5 (mucus cells) were detected by antibody probes (red) to define infected cell types (6 dpi). Scale bar: 10 μm. (D) Human airway epithelial cells (Calu-3) were analyzed with IHC for pYAP127 and SARS-CoV-2 Spike protein (red) in uninfected (Mock)

and infected cells at 48 hours post-infection. Parental and Delta strains were used for infection studies (MOI 0.1). Scale bar: 50 μm. Insets highlight phospho-YAP S127 in infected cells, and white asterisks denote uninfected cells. Representative data from 3 independent studies are provided. ALI, air–liquid interface; COVID-19, Coronavirus Disease 2019; DEG, differentially expressed gene; IHC, immunohistochemistry; KEGG, Kyoto Encyclopedia of Genes and Genomes; MOI, multiplicity of infection; SARS-CoV-2, Severe Acute Respiratory Syndrome Coronavirus 2.

https://doi.org/10.1371/journal.pbio.3001851.g001

is less susceptible to parental SARS-CoV-2 infection [39], we followed the viral infection for up to 6 days. Western blot analysis of protein samples collected at 2 and 6 days post-infection (dpi), showed an increased level of phosphorylated YAP (Ser127) suggesting activation of the Hippo signaling pathway during SARS-CoV-2 infection (Fig 1C). Interestingly, we have noticed an increase in total YAP1 protein level in the infected samples. In addition, we observed a concurrent activation of the innate immune pathway as evidenced by an increase in phosphorylated STAT1 (Tyr701). SARS-CoV-2 infection was confirmed in the lung ALI culture by western blot and immunohistochemistry that revealed both ciliated and mucus secreted cells were infected at 6 dpi (Fig 1C). Next, we examined the Hippo signaling pathway in the Calu-3 human airway epithelial cell line during infection with SARS-CoV-2 parental as well as the Delta variant of concern (VOC) (Fig 1D). We observed that both the parental and Delta variant strains of SARS-CoV-2 increased phospho-YAP (Ser127) level in the infected Calu-3 cell cultures (MOI 0.1). Interestingly, the phospho-YAP (Ser127) protein aggregates formed punctate structures in the cytoplasm, likely for potential degradation in autophagosomes [41]. Taken together, the Hippo signaling pathway is activated in COVID-19 infected lungs and SARS-CoV-2 infected in vitro lung culture systems.

Although SARS-CoV-2 is a major respiratory pathogen, COVID-19 manifestations in the cardiovascular system are also well documented [17,18,42–44]. To further understand how the Hippo signaling pathway may be modulated by SARS-CoV-2 and the host response, we studied this pathway in cardiomyocytes. Human pluripotent stem cell-derived cardiomyocytes (hPSC-CMs) have been shown to be efficient at recapitulating cardiovascular diseases at a cellular level [45,46], have demonstrated susceptibility to SARS-CoV-2 replication [47], and have been used as a platform to study potential therapeutics against SARS-CoV-2 infection [19]. Transcriptomic analysis of SARS-CoV-2-infected hPSC-CM system [48] showed that 25 genes in the Hippo pathway are significantly differentially expressed ($p < 0.01$), of which 19 (76%) of the genes are up-regulated relative to uninfected mock hPSC-CM control (S1B Fig and S4 Data). While comparing the Hippo pathway DEGs of COVID-19 lung samples (Fig 1A and S1 Data) and of hPSC-CMs (S1B Fig and S4 Data), we observed that genes such as BMPR1B and GDF6 are commonly up-regulated. Subsequently, we used these highly susceptible hPSC-CM to further investigate the kinetics of the Hippo signaling pathway during early and late phases of viral infection. SARS-CoV-2-infected cardiomyocytes were confirmed by specific cell-staining of cardiac troponin T (cTnT) and viral Spike proteins (Fig 2A). SARS-CoV-2 induced pronounced cytopathic effect (CPE), characterized by cell fusion and rounding of cells, and fragmentation of cTnT filaments, as well as apoptosis by activation of cleavage of caspase-3 (CC3) indicated the high susceptibility of hPSC-CM to cell death by infection. Western blot revealed that YAP1 is induced at 2 and 24 hpi but degraded by 48 hpi (Fig 2B). Simultaneously, there is an induction of phospho-YAP1 (S127) in the infected cells, which indicate a strong activation of the Hippo signaling pathway. Also, SARS-CoV-2 infection results in increased levels of phospho-TBK1 and phospho-IRF3 indicating activation of the RLR innate immune signaling pathway as early as 2 hpi. In addition, the antiviral STAT1 Type I interferon (IFN) pathway is induced in hPSC-CM following infection (Fig 2B). Incoming viral RNA and envelope glycoprotein can be detected by TLR and RLR-IFN pathway sensors in minutes [49–51], which can allow the cells to mount effective antiviral defense. Furthermore,

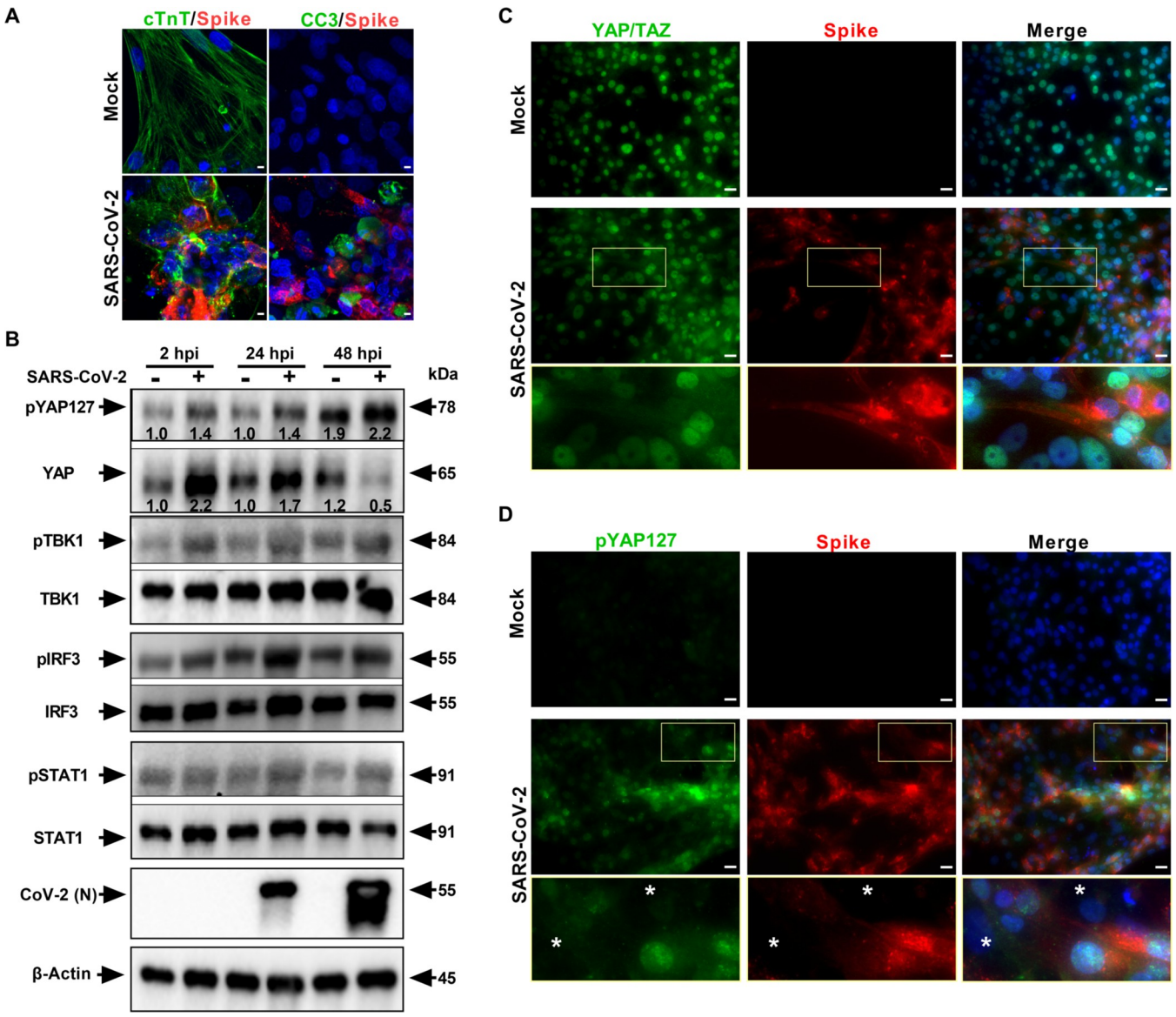

Fig 2. SARS-CoV-2 infection activates Hippo and antiviral RLR-STAT pathways in hPSC-CMs. (A) Confocal image analysis of SARS-CoV-2 Spike protein (red) in infected cardiomyocytes shows extensive damage to cTNT positive (green) cells, which undergo apoptotic cell death (green; cleaved caspase 3). Scale bar: 5 μm; $n = 6$ independent experiments. (B) Western blot analyzes show activation of Hippo, RLR, and STAT1 pathways. Phospho-YAP127 level is increased upon SARS-CoV-2 infection (MOI 0.01); $n = 3$ independent experiments. Density of bands compared to that of 2 hpi mock is provided for pYAP127 and YAP. (C) Immunohistochemistry analysis of SARS-CoV-2 Spike protein in infected hPSC-CMs at 48 hpi reveals cytoplasmic localization and depletion of YAP/TAZ and (D) increase in pYAP127 level. Scale bar: 25 μm. Insets denote total YAP or pYAP127 in infected cells, and white asterisks highlight uninfected cells. hPSC-CM, human pluripotent stem cell-derived cardiomyocyte; MOI, multiplicity of infection; SARS-CoV-2, Severe Acute Respiratory Syndrome Coronavirus 2.

https://doi.org/10.1371/journal.pbio.3001851.g002

immunohistochemical analysis showed that YAP/TAZ has been depleted in the infected cells with a cytoplasmic localization (Fig 2C) and the level of pYAP127 has increased at 48 hpi (Fig 2D). Phosphorylation of YAP at Serine 127 residue by LATS1/2 leads to cytoplasmic distribution of the YAP protein and prevents its transactivation function [52]. Collectively, our data concludes that the Hippo signaling cascade is also active during SARS-CoV-2 infection of cardiomyocyte systems; therefore, we next sought to determine the functional relevance of this pathway.

In order to uncover the functional significance of the Hippo pathway, we utilized both genetic and pharmacological ablation approaches. The core Hippo signaling pathway is a kinase cascade where MST1/2 kinases and Sav1 form a complex to phosphorylate and activate LATS1/2 kinases. After activation, LATS1/2 can phosphorylate and inhibit YAP and TAZ transcription co-activators. YAP/TAZ, when dephosphorylated, interacts with TEAD1-4 and additional transcription factors to stimulate gene expression for cell proliferation and to inhibit apoptosis. Therefore, the Hippo pathway is regulated at multiple levels. MST1/2 and LATS1/2 are regulated upstream by other molecules like Merlin and KIBRA, and YAP/TAZ is regulated downstream by protein ubiquitination. Thus, we postulated that inhibition of MST1/2 and LATS1/2 would lead to an increase in YAP/TAZ activity, and consequently an increase in SARS-CoV-2 replication. To test this mechanism, we performed shRNA-mediated gene silencing experiments in hPSC-CM. For knockdown experiments, we transduced the cells with lentiviral vectors expressing nonspecific control shRNA or shRNAs targeting YAP/TAZ or LATS1. Approximately 72 hours post-transduction, the cells were infected with SARS-CoV-2 at MOI of 0.01. At 48 hpi, the cells were fixed for IHC or harvested in RIPA protein lysis buffer for western blot analysis. Immunohistochemical analysis revealed that the shRNA-mediated partial knockdown of YAP1 gene in hPSC-CM cells resulted in significantly reduced SARS-CoV-2 infection, whereas LATS1 knockdown, increased SARS-CoV-2 infection (Fig 3A and 3D). The quantification of spike antigen positive infected cells is provided in Fig 3D and S2 Data. These observations were also verified at the protein level (Fig 3B). Our observation that the induction of YAP protein at early stages of SARS-CoV-2 infection (Fig 2B) could be due to viral-mediated up-regulation of pro-viral YAP protein as a result of a complex viral–host interaction response and signaling feedback regulation. Taken together, our data provide evidence that the YAP/TAZ is a pro-viral factor, whereas LATS1 has antiviral function.

In addition, we investigated well-characterized direct acting chemical inhibitors on the Hippo signaling pathway. XMU-MP-1 blocks MST1/2 kinase activities and thereby enhances YAP/TAZ activity. MST1 and MST2 are core components of the Hippo pathway and critical targets for tissue repair and regeneration [53]. Therefore, XMU-MP-1, a selective and reversible inhibitor, increases tissue repair and regeneration properties following tissue injuries [53,54]. XMU-MP-1 increases cardiomyocyte survival and reduces apoptosis following oxidative stress [54]. In mice, XMU-MP-1 has been shown to increase intestinal repair, liver repair and regeneration [53], and preserve cardiac function and inhibit cardiomyocyte apoptosis in mice with transverse aortic constriction (TAC) [54]. Infection of cardiomyocytes and Calu-3 lung cells pre-treated with the MST1/2 inhibitor, XMU-MP-1 (10 μm), led to an increase in SARS-CoV-2 replication (Fig 3C–3E). XMU-MP-1 compound is non-toxic to the Calu-3 cells (S2A Fig). Interestingly, XMU-MP-1 treatment induced a coarse granular morphology to the nuclear localized YAP/TAZ (Fig 3E), and in infected cells the YAP/TAZ protein was depleted. Furthermore, XMU-MP1 treatment stimulated an increase in SARS-CoV-2 replication. Similar to the activity of XMU-MP-1, MST1/2 loss of function mutations in humans result in immune deficiency disorders and the affected individuals are more susceptible to human papilloma infections [33]. Consistent with the clinical observation, our study indicates that pharmacological inhibition of MST1/2 promotes the susceptibility of cardiac and lung cells to SARS-CoV-2 infection. Thus, MST1/2 or LATS1/2 loss of function mutations can potentially increase susceptibility to SARS-CoV-2 infections in humans.

Since YAP/TAZ is a proviral factor, pharmacological inhibition can provide additional therapeutic options for COVID-19 treatments. Thus, we focused on pharmacological modulation of YAP/TAZ. Verteporfin, a small molecule derivative of porphyrin, is a YAP-TEAD inhibitor. Verteporfin is a US Food and Drug Administration (FDA) approved drug used in

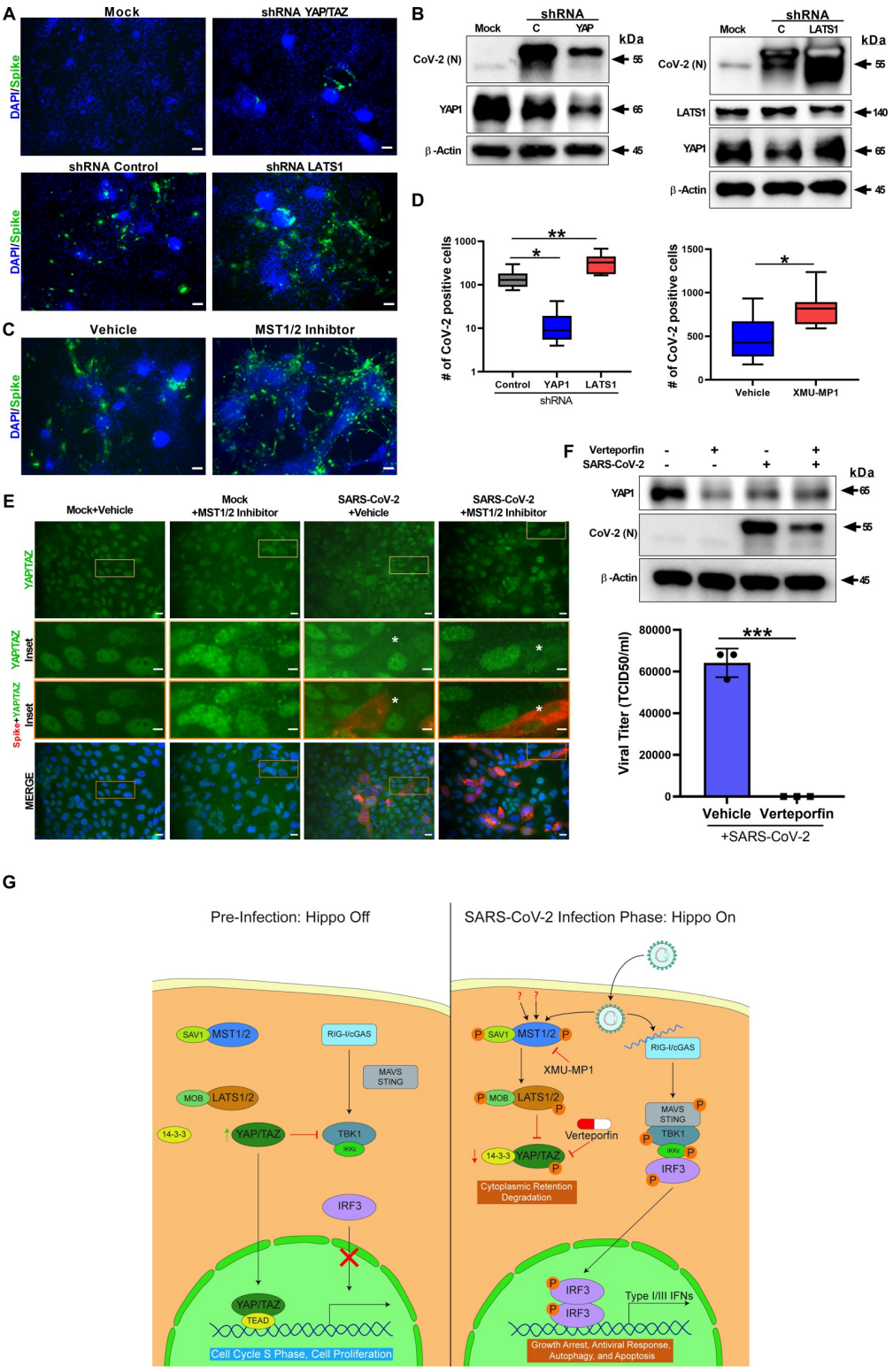

Fig 3. ShRNA-mediated knockdown and pharmacological modulation of SARS-CoV-2 replication. (A) IHC analysis of shRNA-mediated knockdown of YAP1 and LATS1-specific shRNAs showed efficiently reduced or increased SARS-CoV-2 replication (green) relative to shRNA control, respectively, in hPSC-CMs. Scale bar: 50 μm. (B) Western blot analysis of shRNA-mediated knockdown of YAP1 and LATS1 respective protein expression. (Con: Control shRNA). (C) IHC images of XMU-MP-1 (MST1/2 inhibitor) and vehicle-treated hPSC-CMs are shown. Note:

XMU-MP-1 increased SARS-CoV-2 replication (green) in hPSC-CM. (D) Graphs depict quantification of SARS-CoV-2 positive cells in infected hPSC-CM respective to panels A and C. Data represented as the average of technical replicates and SEM. Student *t* test. $^{**}P > 0.001$; $n = 2$ independent experiments. (E) IHC Images show YAP/TAZ protein (green) and SARS-CoV-2 Spike antigen (red) in Calu-3 cells. Note, MST1/2 inhibitor-treated Calu-3 cells have higher number of infected cells. Inset and white asterisk hovers infected cells showing depletion of YAP/TAZ. Scale bar: 25 μm. Inset scale bar: 10 μm. (F) Western blot analysis of Calu-3 cells treated with Verteporfin (1 μm) and SARS-CoV-2 infection. Drug treatment resulted in reduction in SARS-CoV-2 infection. Graph shows the viral titer (TCID50/ml) measurement of infected as well as treated Calu-3 culture supernatant (representative data from 2 independent experiments). (G) Schematic diagram of our hypothetical model integrating Hippo and TBK1 signaling pathways during preinfection (Hippo off) and SARS-CoV-2 infection states (Hippo on). c-GAS, cyclic GMP-AMP synthase; IKKe, inhibitor of nuclear factor kappa B kinase subunit epsilon; MAVS, mitochondrial antiviral-signaling protein; RIG-I, retinoic acid inducible gene I protein; STING, stimulator of interferon response cGAMP interactor 1; TEAD, TEA domain transcription factors. Individual quantitative observations that underlie the data summarized in Fig 3D and 3F can be located under the Supporting Information File as S2 and S3 Data files, respectively. hPSC-CM, human pluripotent stem cell-derived cardiomyocyte; SARS-CoV-2, Severe Acute Respiratory Syndrome Coronavirus 2.

https://doi.org/10.1371/journal.pbio.3001851.g003

patients with predominantly classic, subfoveal choroidal neovascularization (CNV) caused by age-related macular degeneration (AMD) (VAM) [55]. In addition, because YAP is a pro-tumorigenic factor expressed in multiple cancers, Verteporfin has been used to inhibit YAP as an anti-cancer chemotherapeutic and adjuvant drug [56], which increased phosphorylation of YAP1 (S127) in Calu-3 cells (S2B Fig). Therefore, modulating YAP/TAZ with Verteporfin can provide more insight into YAP's proviral properties. Calu-3 cells were pretreated with 1 μm Verteporfin (non-toxic concentration; S2A Fig) for 24 hours and subsequently the cells were infected with SARS-CoV-2. At 48 hpi, the cells were harvested for protein analysis and the culture supernatants were collected for measuring viral titer. Verteporfin treatment resulted in a reduction of YAP/TAZ protein level compared to vehicle-treated cells (Fig 3F and S3 Data) as well as a decrease in SARS-CoV-2 replication at 48 hpi. Viral titer (TCID50/ml) measurement of Verteporfin-treated infected cell culture media revealed there was a significant decrease of viral production in Calu-3 cells (Fig 3F and S3 Data). Our observation supports the results of an independent study that used an FDA-approved drug library of 3,200 small molecules to discover anti-SARS-CoV-2 compounds and identified Verteporfin and verified its antiviral properties in a mouse model [57]. Together, our results indicate a direct antiviral role of Hippo signaling on SARS-CoV-2 infection and disease pathogenesis processes, which can be therapeutically targeted. A schematic diagram of our working hypothetical model is shown in Fig 3G.

In conclusion, our results show that SARS-CoV-2 infection caused activation of the Hippo signaling pathway in hPSC-CMs, human primary lung ALI cultures, and human airway epithelial cells (Calu-3). These in vitro cultures are efficiently infected by SARS-CoV-2, consequently causing activation of immune, and inflammatory responses, and altered Hippo signaling cascade. shRNA-mediated partial knockdown of LATS1 and pharmacological modulation of core upstream MST1/2 kinases resulted in enhanced SARS-CoV-2 replication. Loss of function mutations in these antiviral kinases could enhance susceptibility to SARS-CoV-2 infections in human. While Verteporfin, a pharmacological inhibitor targeting downstream transactivator, YAP, significantly reduced viral replication and production. Moving forward, additional mechanistic investigations are required to elucidate the underpinnings of the Hippo pathway role in antiviral responses across pandemic potential RNA viruses and additional preclinical small and large animal safety and efficacy studies of Verteporfin therapy for COVID-19. Taken together, our results indicate a direct antiviral role for Hippo signaling in SARS--CoV-2 infection, thus creating potentially new avenues this pathway can be pharmacologically targeted to treat COVID-19.

Methods/Materials

Ethics statement

Our study does not involve human subjects, but used deidentified human tissues. For human tissue procurement, large airways and bronchial tissues were acquired after lung transplantations at the Ronald Reagan UCLA Medical Center from deidentified normal human donors following Institutional Review Board [58] exemption. Pluripotent stem cell-related work received UCLA ESCRO-IRB approval. All the SARS-CoV-2 live virus experiments were performed at the UCLA BSL3 High containment facility.

Cell lines, hPSC-CM cultures, and ALI cultures

Vero E6 cells were obtained from ATCC [VERO C1008 (ATCC CRL-1586)] or DSMZ (Braunschweig, Germany). Cells were cultured in EMEM growth media containing 10% fetal bovine serum (FBS) and penicillin (100 units/ml). Human lung adenocarcinoma epithelial cell line (Calu-3) was purchased from ATCC (ATCCHTB-55) and cultured in Dulbecco's Modified Eagles Medium (DMEM), supplemented with 20% FBS, 1% L-glutamine (L-glu), and 1% penicillin/streptomycin (P/S). Cells were incubated at 37˚C with 5% CO_2. hPSC-CMs were derived from hESC line H9 using the previously described method [59]. Temporarily, hPSCs were maintained in mTeSR1 (STEMCELL Technology). Shortly after, RPMI1640 was supplemented with B27 minus insulin (Invitrogen) and used as differentiation medium. From Day 0 to 1, 6 μm CHIR99021 (Selleckchem) was added into differentiation medium. Next, Day 3 to 5, 5 μm IWR1 (Sigma-Aldrich) was added to differentiation medium. After Day 7, RPMI 1640 plus B27 maintenance medium was added. From Day 10 to 11, RPMI 1640 without D-glucose supplemented with B27 was transiently used for metabolic purification of CMs [60]. After selection, hPSC-CMs were replated for viral infection. ALI cultures derived from primary human proximal ABSCs were used as described previously [40]. The 24-well 6.5-mm transwells with 0.4-mm pore polyester membrane inserts were used for culturing ALI cells. A total of 500 μl ALI media (PneumaCult-ALI Medium, STEMCELL Technologies) was used in the basal chamber for ALI cultures, and cells were cultured at 37˚C with 5% CO_2. Use of these established cell lines for the study was approved by the Institutional Biosafety Committee at UCLA.

shRNA-mediated gene silencing

hPSC-CM cells (1×10^5 cells/well) were added in a 48-well plate. The pLKO.1-puro sh-RNA targeting YAP1 (5′-CCGGCCCAGTTAAATGTTCACCAATCTCGAGATTGGTGAACATTTAACTGGGTTTTTG-3′), LATS1 (5′-CCGGCAAGTCAGAAATCCACCCAAACTCGAGTTTGGGTGGATTTCTGACTTGTTTTT—3′) or pLKO.1-puro Non-Targeting shRNA Control (Sigma-Aldrich) lentiviral particles were added to the cells. At 72 hours post-transduction, SARS-CoV-2 (Isolate USA-WA1/2020) with a multiplicity of infection (MOI) of 0.01 was added. At 48 hours post-infection, cells were fixed in 4% paraformaldehyde for IHC studies or cell protein lysates were collected for western blot analysis.

Pharmacological modulation of Hippo signaling pathway in infected cells

hPSC-CM and Calu-3 cells were seeded on 48-well plates or 96-well plates, respectively. hPSC-CM cells were pretreated with 4-((5,10-dimethyl-6-oxo-6,10-dihydro-5H-pyrimido[5,4-b]thieno[3,2-e][1,4]diazepin-2-yl)amino)benzenesulfonamide (XMU-MP-1 at 10 μm) and Calu-3 cells were treated with XMU-MP-1 (10 μm) or Verteporfin (1 μm). Cells were pretreated with drugs for 24 hours, then infected with SARS-CoV-2 inoculum (MOI 0.1). DMSO

vehicle-treated cells, with or without viral infections, were included as controls. At 48 hpi, the cells were fixed with 4% PFA or lysed with RIPA buffer for proteins. The cell-free culture supernatants were collected from Calu-3 for viral titer measurement. Fixed cells were immunostained with anti-spike antibody (NR-616 Monoclonal Antibody) to assess virus replication.

Virus

SARS-Related Coronavirus 2 (SARS-CoV-2), Isolate USA-WA1/2020, and Isolate hCoV-19/USA/MD-HP05647/2021 (Lineage B.1.617.2; Delta variant) were obtained from BEI Resources of National Institute of Allergy and Infectious Diseases (NIAID). All the studies involving live virus was conducted in UCLA BSL3 high-containment facility. SARS-CoV-2 was passaged once in Vero E6 cells and viral stocks were aliquoted and stored at −80˚C. Virus titer was measured in Vero E6 cells by established plaque assay or TCID50 assay.

SARS-CoV-2 infection

Calu-3 cells were seeded at 30×10^3 cells per well in 0.2 ml volumes using a 96-well plate and hPSC-CMs were replated at 1×10^5 cells per well in a 48-well plate. Viral inoculum (MOI of 0.01 or 0.1; 100 μl/well) was added using serum-free base media. The conditioned media from each well and condition was removed and 100 μl of prepared inoculum was added onto cells. After 1 hour incubation at 37˚C with 5% CO2, inoculum was replaced for Calu-3 cells with serum-supplemented media (200 μl per well) and for hPSC-CM, cell culture medium was replaced with RPMI 1640 + B27 supplement with insulin. In all our experiments, we included 48 hpi as a standard endpoint unless otherwise stated. For ALI cultures, 100 μl of viral inoculum (MOI of 1) prepared in PneumaCult media was added to the apical chamber of ALI culture insert and incubated for 1 hour at 37˚C with 5% CO2. For mock infection, PneumaCult media (100 μl/well) alone was added. The inoculum was dispersed throughout the hour every 15 minutes by gently tilting the plate sideways. At the end of incubation, the inoculum was removed from the apical side for ALI cultures to maintain the ALI [19,40]. At selected time points, cells were fixed with 4% PFA, collected by 1xRIPA for protein analysis, and/or supernatant collected for viral titer. Viral infection was examined by immunostaining or western blot analysis using SARS-CoV-2 antibodies. BEI Resources NR-616 monoclonal anti-SARS-CoV Spike protein (Similar to 240C) SARS coronavirus for immunostaining and GeneTex SARS--CoV-2 (COVID-19) Nucleocapsid antibody [HL344] (Cat#GTX635679) for western blot.

Viral titer by TCID50 (median tissue culture infectious dose) assay

Viral production by infected cells was measured by quantifying TCID50 as previously described [61] methodology for quantifying TCID50; 10×10^3 cells/well of Vero E6 cells were seeded in 96-well plates. The next day, culture media samples of supernatant collected from Calu-3 cells were at 48-hour time point was subjected to 10-fold serial dilutions (10^1 to 10^8) and inoculated onto Vero E6 cells. The cells were incubated at 37˚C with 5% CO2 for 3 to 4 days to evaluate for presence or absence of viral CPE. After measuring the percent infected dilutions immediately above and immediately below 50%, the TCID50 was calculated based on the method of Reed and Muench.

Histopathology

COVID-19 patient autopsy lung samples and normal lung samples ($n = 4$ each) were procured from the UCLA Translational Pathology Core Lab for research use. Samples were processed and sectioned, after a pathologist confirmed the section quality by H&E staining, and

subsequent confirmation of COVID-19 positivity by RNAscope V-nCoV2019-S probe (ACD, Cat#: 848568, ready to use). Immunohistochemistry stainings were also performed on this lung tissue: Paraffin-embedded sections were cut at 4-μm thickness and paraffin was removed with xylene and the sections were rehydrated through graded ethanol. Endogenous peroxidase activity was blocked with 3% hydrogen peroxide in methanol for 10 minutes. Heat-induced antigen retrieval [9] was carried out for all sections in AR9 buffer (AR9001KT Akoya) using a Biocare decloaker at 95˚C for 25 minutes. The slides were then stained with YAP (S127) antibody (Cell Signaling, 13008, 1–100) and CD68 antibody (Dako, m0876, 1–200) at 4 degree overnight; the signal was detected using Bond Polymer Refine Detection Kit (Leica Microsystems, catalogue #DS9800) with a diaminobenzidine reaction to detect antibody labeling and hematoxylin counterstaining.

Immunohistochemistry

Cells were fixed with 4% PFA for 30 to 60 minutes or methanol (incubated in −20˚C freezer until washed with 1XPBS). Cells were washed 3 times with 1× PBS before permeabilizing with blocking buffer (0.3% Triton X-100, 2% BSA, 5% Goat Serum, 5% Donkey Serum in 1× PBS) for 1 hour at room temperature. After adding specific primary antibodies (refer to S1 Table), cells were incubated overnight at 4˚C. The next day, cells were washed with 1× PBS 3 times and incubated with respective secondary antibody (refer to S1 Table) at room temperature for 1 hour. DAPI (4′,6-diamidino-2-phenylindole, dihydrochloride) (Life Technologies) was used to stain nuclei at a dilution of 1:5,000 in 1× PBS. Image acquisition was done using Leica DMi1 fluorescent microscopes and using the Leica Application Suite X (LAS X). The LSM 700 confocal microscopes and Zeiss Software programs available at the UCLA Eli and Edythe Broad Center of Regenerative Medicine and Stem Cell Research Microscopy Core at Center for Health Sciences Building was used for capturing images as well.

Western blot analysis

Cells were lysed in 1× RIPA 50 mM Tris (pH 7.4), 1% NP-40, 0.25% sodium deoxycholate, 1 mM EDTA, 150 mM NaCl, 1 mM Na3VO4, 20 Mm or NaF, 1 mM PMSF, 2 mg ml^{-1} aprotinin, 2 mg ml^{-1} leupeptin and 0.7 mg ml^{-1} pepstatin or Laemmli Sample Buffer (Bio Rad, Hercules, California, United States of America). Cell lysates were resolved by SDS-PAGE using 10% gradient gels and transferred to a 0.2 μm PVDF membrane. Subsequently, the membranes were blocked with 5% skim milk and 0.1% Tween-20 in 1× TBST (0.1% Tween-20) at room temperature for 1 hour. The membranes were then probed with respective monoclonal antibodies and detected by Thermo Scientific SuperSignal West Femto Maximum Sensitivity Substrate.

Image analysis/quantification

The confocal images were obtained using the Leica Application Suite X (LAS X) and/or the Zeiss LSM 700 Confocal Microscopy by Zeiss Software Program with maximum intensity projection feature. Using a double-blinded approach to count the positively stained cells, Image J's plugin Cell Counter program was used. Approximately 3 to 4 independent images per condition of the hPSC-CM were analyzed. For all the analysis, we used confocal images acquired at 63× objective and fluorescent microscope images acquired at 20 and 40×. Total number of cells in each image was obtained by manually counting all the DAPI-stained nuclei using ImageJ program (Version 1.8.0; https://imagej.nih.gov/ij/index.html). Total cell count was then used for normalization and to calculate the percentage of individual marker positive cell

populations in respective images. The mean percentage of positively stained cells from 3 to 8 independent images (about 150 to 1,000 cells total) were quantified and presented as graph format.

RNA sequencing data analysis

We used a previously published [38] RNA sequencing dataset of 5 normal and autopsy lung samples from COVID-19 patients were obtained from the NCBI Gene Expression Omnibus (GEO) under the accession number GSE150316 [38]. The SARS-CoV-2 infected pluripotent stem cell-derived cardiomyocytes gene expression data used in this study were also retrieved from GEO under the accession number GSE150392 [47]. The raw read counts per gene were used as inputs for differential expression gene analysis using DESeq2 v1.28.1 in R v4.0.3 [62]. Median of ratios method was used to normalize expression counts for each gene in all experimental samples. Each gene in the samples was fitted into a negative binomial generalized linear model. Genes were considered as differentially expressed (DEG) if they were supported by a false discovery rate (FDR) $p < 0.01$. The heatmaps were prepared using shinyheatmap web interface [63], which uses normalized read counts as inputs for Z-score normalization, which is computed on a gene-by-gene basis by subtracting the mean and then dividing by the standard deviation. The KEGG pathway database was used to examine the hippo signaling pathway in the DEG datasets [64].

Data analysis

All statistical testing was performed at the 2-sided alpha level of 0.05. To test statistical significance, unpaired Student *t* test was used to compare 2 groups (uninfected versus infected). GraphPad Prism software, version 8.1.2 (GraphPad Software, US) was used.

Supporting information

S1 Fig. (A) Immunohistochemistry of COVID-19 lung autopsy tissue shows heavy infiltration of CD68-positive inflammatory cells (red) (scale bar: 100 μm). (B) Heatmap depicting Z scores as expression levels of the 25 differentially expressed genes ($p < 0.01$) involved in Hippo signaling pathway of SARS-CoV-2-infected hPSC-cardiomyocytes relative to uninfected cells at 3 dpi. Blue and red colors represent 6 down-regulated and 19 up-regulated genes, respectively. These differentially expressed genes in the Hippo signaling pathway were identified using the KEGG pathway database. The gene expression data was retrieved at Gene Expression Omnibus with accession number GSE150392. Individual quantitative observations that underlie the data summarized can be located under the Supporting Information File as S4 Data.
(TIF)

S2 Fig. (A) Graph shows the percent cytotoxicity of Calu-3 cells 72 hours post-treatment with DMSO (Vehicle), XMU-MP1 (10 μm), and Verteporfin (1 μm). CellTiter-Glo Luminescent Cell Viability Assay was performed as per the manufacturer (Promega, USA) recommendation. Individual quantitative observations that underlie the data summarized can be located under the Supporting Information File as S5 Data. (B) Western blot analysis shows total and phosphorylated YAP at 72 hours post treatment with indirect and direct acting inhibitors, XMU-MP-1 and Verteporfin, respectively. Note: XMU-MP-1 treatment enhances YAP/TAZ level compared to vehicle, whereas Verteporfin increases phosphorylated YAP (S127) levels. Representative data from 2 independent experiments is shown.
(TIF)

S1 Table. Reagents or resources used in this study.
(DOCX)

S1 Raw Material. Blot-gel data file.
(PDF)

S1 Data. Raw data file for Fig 1A.
(XLSX)

S2 Data. Raw data file for Fig 3D.
(XLSX)

S3 Data. Raw data file for Fig 3F.
(XLSX)

S4 Data. Raw data file for S1B Fig.
(XLSX)

S5 Data. Raw data file for S2A Fig.
(XLSX)

Acknowledgments

We are grateful to Barbara Dillon, UCLA High Containment Program Director for BSL3 work. We thank Nate Price for assistance with manuscript editing and proofreading, and Nikhil Chakravarty for design and production of illustrations. The following reagents were obtained through BEI Resources, NIAID, NIH: Monoclonal Anti-SARS-CoV S Protein (Similar to 240C); SARS-Related Coronavirus 2, Isolate USA-WA1/2020, (NR-52281); SARS-CoV-2, Isolate hCoV-19/USA/PHC658/2021 (Delta Variant) (NR-55611).

Author Contributions

Conceptualization: Gustavo Garcia, Jr., Arunachalam Ramaiah, Vaithilingaraja Arumugaswami.

Data curation: Gustavo Garcia, Jr., Arjit Vijey Jeyachandran, Yijie Wang, Joseph Ignatius Irudayam, Sebastian Castillo Cario, Chandani Sen, Shen Li, Yunfeng Li, Ashok Kumar, Karin Nielsen-Saines, Samuel W. French, Priya S. Shah, Kouki Morizono, Brigitte N. Gomperts, Arjun Deb, Arunachalam Ramaiah, Vaithilingaraja Arumugaswami.

Formal analysis: Gustavo Garcia, Jr., Arjit Vijey Jeyachandran, Yijie Wang, Joseph Ignatius Irudayam, Sebastian Castillo Cario, Chandani Sen, Shen Li, Yunfeng Li, Ashok Kumar, Karin Nielsen-Saines, Samuel W. French, Priya S. Shah, Kouki Morizono, Brigitte N. Gomperts, Arjun Deb, Arunachalam Ramaiah, Vaithilingaraja Arumugaswami.

Funding acquisition: Arjun Deb, Vaithilingaraja Arumugaswami.

Investigation: Gustavo Garcia, Jr., Arunachalam Ramaiah, Vaithilingaraja Arumugaswami.

Project administration: Vaithilingaraja Arumugaswami.

Resources: Vaithilingaraja Arumugaswami.

Supervision: Vaithilingaraja Arumugaswami.

Validation: Brigitte N. Gomperts, Arunachalam Ramaiah, Vaithilingaraja Arumugaswami.

Visualization: Vaithilingaraja Arumugaswami.

Writing – original draft: Gustavo Garcia, Jr., Arjit Vijey Jeyachandran, Yijie Wang, Joseph Ignatius Irudayam, Sebastian Castillo Cario, Chandani Sen, Shen Li, Yunfeng Li, Ashok Kumar, Karin Nielsen-Saines, Samuel W. French, Priya S. Shah, Kouki Morizono, Brigitte N. Gomperts, Arunachalam Ramaiah, Vaithilingaraja Arumugaswami.

Writing – review & editing: Gustavo Garcia, Jr.

References

1. Ramaiah A, Arumugaswami V. Insights into Cross-species Evolution of Novel Human Coronavirus 2019-nCoV and Defining Immune Determinants for Vaccine Development. bioRxiv. 2020:2020.01.29.925867.
2. Wu F, Zhao S, Yu B, Chen Y-M, Wang W, Song Z-G, et al. A new coronavirus associated with human respiratory disease in China. Nature. 2020; 579(7798):265–269. https://doi.org/10.1038/s41586-020-2008-3 PMID: 32015508
3. Zhou P, Yang X-L, Wang X-G, Hu B, Zhang L, Zhang W, et al. A pneumonia outbreak associated with a new coronavirus of probable bat origin. Nature. 2020; 579(7798):270–273. https://doi.org/10.1038/s41586-020-2012-7 PMID: 32015507
4. Xu H, Zhong L, Deng J, Peng J, Dan H, Zeng X, et al. High expression of ACE2 receptor of 2019-nCoV on the epithelial cells of oral mucosa. Int J Oral Sci. 2020; 12(1):8. https://doi.org/10.1038/s41368-020-0074-x PMID: 32094336
5. Wang K, Chen W, Zhang Z, Deng Y, Lian JQ, Du P, et al. CD147-spike protein is a novel route for SARS-CoV-2 infection to host cells. Signal Transduct Target Ther. 2020; 5(1):283. https://doi.org/10.1038/s41392-020-00426-x PMID: 33277466
6. Wang S, Qiu Z, Hou Y, Deng X, Xu W, Zheng T, et al. AXL is a candidate receptor for SARS-CoV-2 that promotes infection of pulmonary and bronchial epithelial cells. Cell Res. 2021; 31(2):126–140. https://doi.org/10.1038/s41422-020-00460-y PMID: 33420426
7. Cantuti-Castelvetri L, Ojha R, Pedro LD, Djannatian M, Franz J, Kuivanen S, et al. Neuropilin-1 facilitates SARS-CoV-2 cell entry and infectivity. Science (New York, NY). 2020; 370(6518):856–860. https://doi.org/10.1126/science.abd2985 PMID: 33082293
8. Daly JL, Simonetti B, Klein K, Chen KE, Williamson MK, Anton-Plagaro C, et al. Neuropilin-1 is a host factor for SARS-CoV-2 infection. Science (New York, NY). 2020; 370(6518):861–865. https://doi.org/10.1126/science.abd3072 PMID: 33082294
9. Hoffmann M, Kleine-Weber H, Schroeder S, Kruger N, Herrler T, Erichsen S, et al. SARS-CoV-2 Cell Entry Depends on ACE2 and TMPRSS2 and Is Blocked by a Clinically Proven Protease Inhibitor. Cell. 2020. https://doi.org/10.1016/j.cell.2020.02.052 PMID: 32142651
10. Kai H, Kai M. Interactions of coronaviruses with ACE2, angiotensin II, and RAS inhibitors-lessons from available evidence and insights into COVID-19. Hypertens Res. 2020; 43(7):648–654. https://doi.org/10.1038/s41440-020-0455-8 PMID: 32341442
11. Chakravarty N, Senthilnathan T, Paiola S, Gyani P, Castillo Cario S, Urena E, et al. Neurological pathophysiology of SARS-CoV-2 and pandemic potential RNA viruses: a comparative analysis. FEBS Lett. 2021; 595(23):2854–2871. https://doi.org/10.1002/1873-3468.14227 PMID: 34757622
12. Pacciarini F, Ghezzi S, Canducci F, Sims A, Sampaolo M, Ferioli E, et al. Persistent replication of severe acute respiratory syndrome coronavirus in human tubular kidney cells selects for adaptive mutations in the membrane protein. J Virol. 2008; 82(11):5137–5144. https://doi.org/10.1128/JVI.00096-08 PMID: 18367528
13. Fanelli V, Fiorentino M, Cantaluppi V, Gesualdo L, Stallone G, Ronco C, et al. Acute kidney injury in SARS-CoV-2 infected patients. Crit Care. 2020; 24(1):155. https://doi.org/10.1186/s13054-020-02872-z PMID: 32299479
14. Puelles VG, Lütgehetmann M, Lindenmeyer MT, Sperhake JP, Wong MN, Allweiss L, et al. Multiorgan and Renal Tropism of SARS-CoV-2. N Engl J Med. 2020; 383(6):590–592. https://doi.org/10.1056/NEJMc2011400 PMID: 32402155
15. Varga Z, Flammer AJ, Steiger P, Haberecker M, Andermatt R, Zinkernagel AS, et al. Endothelial cell infection and endotheliitis in COVID-19. Lancet (London, England). 2020; 395(10234):1417–1418. https://doi.org/10.1016/S0140-6736(20)30937-5 PMID: 32325026
16. Yancy CW, Fonarow GC. Coronavirus Disease 2019 (COVID-19) and the Heart—Is Heart Failure the Next Chapter? JAMA Cardiology. 2020.

17. Shi S, Qin M, Shen B, Cai Y, Liu T, Yang F, et al. Association of Cardiac Injury With Mortality in Hospitalized Patients With COVID-19 in Wuhan, China. JAMA Cardiol. 2020; 5(7):802–810. https://doi.org/10.1001/jamacardio.2020.0950 PMID: 32211816

18. Fried JA, Ramasubbu K, Bhatt R, Topkara VK, Clerkin KJ, Horn E, et al. The Variety of Cardiovascular Presentations of COVID-19. Circulation. 2020; 141(23):1930–1936. https://doi.org/10.1161/CIRCULATIONAHA.120.047164 PMID: 32243205

19. Garcia G Jr, Sharma A, Ramaiah A, Sen C, Purkayastha A, Kohn DB, et al. Antiviral drug screen identifies DNA-damage response inhibitor as potent blocker of SARS-CoV-2 replication. Cell Rep. 2021; 35 (1):108940. https://doi.org/10.1016/j.celrep.2021.108940 PMID: 33784499

20. Garcia G Jr, Paul S, Beshara S, Ramanujan VK, Ramaiah A, Nielsen-Saines K, et al. Hippo Signaling Pathway Has a Critical Role in Zika Virus Replication and in the Pathogenesis of Neuroinflammation. Am J Pathol. 2020; 190(4):844–861. https://doi.org/10.1016/j.ajpath.2019.12.005 PMID: 32035058

21. Yamauchi T, Moroishi T. Hippo Pathway in Mammalian Adaptive Immune System. Cell. 2019; 8(5):398. https://doi.org/10.3390/cells8050398 PMID: 31052239

22. Li Z, Zhao B, Wang P, Chen F, Dong Z, Yang H, et al. Structural insights into the YAP and TEAD complex. Genes Dev. 2010; 24(3):235–240. https://doi.org/10.1101/gad.1865810 PMID: 20123905

23. Harvey K, Tapon N. The Salvador-Warts-Hippo pathway—an emerging tumour-suppressor network. Nat Rev Cancer. 2007; 7(3):182–191. https://doi.org/10.1038/nrc2070 PMID: 17318211

24. Meng Z, Moroishi T, Guan KL. Mechanisms of Hippo pathway regulation. Genes Dev. 2016; 30(1):1–17. https://doi.org/10.1101/gad.274027.115 PMID: 26728553

25. Lee DH, Park JO, Kim TS, Kim SK, Kim TH, Kim MC, et al. LATS-YAP/TAZ controls lineage specification by regulating TGFbeta signaling and Hnf4alpha expression during liver development. Nat Commun. 2016; 7:11961.

26. Zhou D, Zhang Y, Wu H, Barry E, Yin Y, Lawrence E, et al. Mst1 and Mst2 protein kinases restrain intestinal stem cell proliferation and colonic tumorigenesis by inhibition of Yes-associated protein (Yap) overabundance. Proc Natl Acad Sci U S A. 2011; 108(49):E1312–E1320. https://doi.org/10.1073/pnas.1110428108 PMID: 22042863

27. Zhao B, Li L, Lei Q, Guan KL. The Hippo-YAP pathway in organ size control and tumorigenesis: an updated version. Genes Dev. 2010; 24(9):862–874. https://doi.org/10.1101/gad.1909210 PMID: 20439427

28. Moroishi T, Hayashi T, Pan WW, Fujita Y, Holt MV, Qin J, et al. The Hippo Pathway Kinases LATS1/2 Suppress Cancer Immunity. Cell. 2016; 167(6):1525–39 e17. https://doi.org/10.1016/j.cell.2016.11.005 PMID: 27912060

29. Janse van Rensburg HJ, Azad T, Ling M, Hao Y, Snetsinger B, Khanal P, et al. The Hippo pathway component TAZ promotes immune evasion in human cancer through PD-L1. Cancer Res. 2018. https://doi.org/10.1158/0008-5472.CAN-17-3139 PMID: 29339539

30. Katagiri K, Katakai T, Ebisuno Y, Ueda Y, Okada T, Kinashi T. Mst1 controls lymphocyte trafficking and interstitial motility within lymph nodes. EMBO J. 2009; 28(9):1319–1331. https://doi.org/10.1038/emboj.2009.82 PMID: 19339990

31. Boro M, Singh V, Balaji KN. Mycobacterium tuberculosis-triggered Hippo pathway orchestrates CXCL1/2 expression to modulate host immune responses. Sci Rep. 2016; 6:37695. https://doi.org/10.1038/srep37695 PMID: 27883091

32. Mou F, Praskova M, Xia F, Van Buren D, Hock H, Avruch J, et al. The Mst1 and Mst2 kinases control activation of rho family GTPases and thymic egress of mature thymocytes. J Exp Med. 2012; 209 (4):741–759. https://doi.org/10.1084/jem.20111692 PMID: 22412158

33. Crequer A, Picard C, Patin E, D'Amico A, Abhyankar A, Munzer M, et al. Inherited MST1 deficiency underlies susceptibility to EV-HPV infections. PLoS ONE. 2012; 7(8):e44010. https://doi.org/10.1371/journal.pone.0044010 PMID: 22952854

34. Zhang Q, Meng F, Chen S, Plouffe SW, Wu S, Liu S, et al. Hippo signalling governs cytosolic nucleic acid sensing through YAP/TAZ-mediated TBK1 blockade. Nat Cell Biol. 2017; 19(4):362–374. https://doi.org/10.1038/ncb3496 PMID: 28346439

35. Abdollahpour H, Appaswamy G, Kotlarz D, Diestelhorst J, Beier R, Schaffer AA, et al. The phenotype of human STK4 deficiency. Blood. 2012; 119(15):3450–3457. https://doi.org/10.1182/blood-2011-09-378158 PMID: 22294732

36. Nehme NT, Schmid JP, Debeurme F, Andre-Schmutz I, Lim A, Nitschke P, et al. MST1 mutations in autosomal recessive primary immunodeficiency characterized by defective naive T-cell survival. Blood. 2012; 119(15):3458–3468. https://doi.org/10.1182/blood-2011-09-378364 PMID: 22174160

37. Du X, Shi H, Li J, Dong Y, Liang J, Ye J, et al. Mst1/Mst2 regulate development and function of regulatory T cells through modulation of Foxo1/Foxo3 stability in autoimmune disease. J Immunol. 2014; 192 (4):1525–1535. https://doi.org/10.4049/jimmunol.1301060 PMID: 24453252

38. Desai N, Neyaz A, Szabolcs A, Shih AR, Chen JH, Thapar V, et al. Temporal and spatial heterogeneity of host response to SARS-CoV-2 pulmonary infection. Nat Commun. 2020; 11(1):6319. https://doi.org/10.1038/s41467-020-20139-7 PMID: 33298930

39. Mulay A, Konda B, Garcia G Jr, Yao C, Beil S, Villalba JM, et al. SARS-CoV-2 infection of primary human lung epithelium for COVID-19 modeling and drug discovery. Cell Rep. 2021; 35(5):109055. https://doi.org/10.1016/j.celrep.2021.109055 PMID: 33905739

40. Purkayastha A, Sen C, Garcia G Jr, Langerman J, Shia DW, Meneses LK, et al. Direct Exposure to SARS-CoV-2 and Cigarette Smoke Increases Infection Severity and Alters the Stem Cell-Derived Airway Repair Response. Cell Stem Cell. 2020; 27(6):869–75.e4. https://doi.org/10.1016/j.stem.2020.11.010 PMID: 33259798

41. Zhao B, Wei X, Li W, Udan RS, Yang Q, Kim J, et al. Inactivation of YAP oncoprotein by the Hippo pathway is involved in cell contact inhibition and tissue growth control. Genes Dev. 2007; 21(21):2747–2761. https://doi.org/10.1101/gad.1602907 PMID: 17974916

42. Dolhnikoff M, Ferreira Ferranti J, de Almeida Monteiro RA, Duarte-Neto AN, Soares Gomes-Gouvêa M, Viu Degaspare N, et al. SARS-CoV-2 in cardiac tissue of a child with COVID-19-related multisystem inflammatory syndrome. Lancet Child Adolesc Health. 2020; 4(10):790–794. https://doi.org/10.1016/S2352-4642(20)30257-1 PMID: 32828177

43. Gnecchi M, Moretti F, Bassi EM, Leonardi S, Totaro R, Perotti L, et al. Myocarditis in a 16-year-old boy positive for SARS-CoV-2. Lancet. 2020; 395(10242):e116. https://doi.org/10.1016/S0140-6736(20)31307-6 PMID: 32593338

44. Escher F, Pietsch H, Aleshcheva G, Bock T, Baumeier C, Elsaesser A, et al. Detection of viral SARS-CoV-2 genomes and histopathological changes in endomyocardial biopsies. ESC Heart Failure. 2020; 7(5):2440–2447. https://doi.org/10.1002/ehf2.12805 PMID: 32529795

45. Lan F, Lee AS, Liang P, Sanchez-Freire V, Nguyen PK, Wang L, et al. Abnormal calcium handling properties underlie familial hypertrophic cardiomyopathy pathology in patient-specific induced pluripotent stem cells. Cell Stem Cell. 2013; 12(1):101–113. https://doi.org/10.1016/j.stem.2012.10.010 PMID: 23290139

46. Sun N, Yazawa M, Liu J, Han L, Sanchez-Freire V, Abilez OJ, et al. Patient-specific induced pluripotent stem cells as a model for familial dilated cardiomyopathy. Sci Transl Med. 2012; 4(130):130ra47–ra47. https://doi.org/10.1126/scitranslmed.3003552 PMID: 22517884

47. Sharma A, Garcia G, Arumugaswami V, Svendsen CN. Human iPSC-Derived Cardiomyocytes are Susceptible to SARS-CoV-2 Infection. Cell Rep Med. 2020.

48. Sharma A, Garcia G, Wang Y, Plummer JT, Morizono K, Arumugaswami V, et al. Human iPSC-Derived Cardiomyocytes Are Susceptible to SARS-CoV-2 Infection. Cell Rep Med. 2020; 1(4):100052. https://doi.org/10.1016/j.xcrm.2020.100052 PMID: 32835305

49. Li Y-G, Siripanyaphinyo U, Tumkosit U, Noranate N, A-nuegoonpipat A, Pan Y, et al. Poly (I:C), an agonist of toll-like receptor-3, inhibits replication of the Chikungunya virus in BEAS-2B cells. Virol J. 2012; 9 (1):114.

50. Kumar A, Zhang J, Yu FS. Toll-like receptor 3 agonist poly(I:C)-induced antiviral response in human corneal epithelial cells. Immunology. 2006; 117(1):11–21. https://doi.org/10.1111/j.1365-2567.2005.02258.x PMID: 16423036

51. Kato H, Takeuchi O, Sato S, Yoneyama M, Yamamoto M, Matsui K, et al. Differential roles of MDA5 and RIG-I helicases in the recognition of RNA viruses. Nature. 2006; 441(7089):101–105. https://doi.org/10.1038/nature04734 PMID: 16625202

52. Moon S, Kim W, Kim S, Kim Y, Song Y, Bilousov O, et al. Phosphorylation by NLK inhibits YAP-14-3-3-interactions and induces its nuclear localization. EMBO Rep. 2017; 18(1):61–71. https://doi.org/10.15252/embr.201642683 PMID: 27979972

53. Fan F, He Z, Kong LL, Chen Q, Yuan Q, Zhang S, et al. Pharmacological targeting of kinases MST1 and MST2 augments tissue repair and regeneration. Sci Transl Med. 2016; 8(352):352ra108. https://doi.org/10.1126/scitranslmed.aaf2304 PMID: 27535619

54. Triastuti E, Nugroho AB, Zi M, Prehar S, Kohar YS, Bui TA, et al. Pharmacological inhibition of Hippo pathway, with the novel kinase inhibitor XMU-MP-1, protects the heart against adverse effects during pressure overload. Br J Pharmacol. 2019; 176(20):3956–3971. https://doi.org/10.1111/bph.14795 PMID: 31328787

55. Bessler NM. Verteporfin therapy in age-related macular degeneration (VAM): an open-label multicenter photodynamic therapy study of 4,435 patients. Retina (Philadelphia, Pa). 2004; 24(4):512–520. https://doi.org/10.1097/00006982-200408000-00003 PMID: 15300071

56. Wei C, Li X. The Role of Photoactivated and Non-Photoactivated Verteporfin on Tumor. Front Pharmacol. 2020; 11:557429. https://doi.org/10.3389/fphar.2020.557429 PMID: 33178014

57. Gu C, Wu Y, Guo H, Zhu Y, Xu W, Wang Y, et al. Protoporphyrin IX and verteporfin potently inhibit SARS-CoV-2 infection in vitro and in a mouse model expressing human ACE2. Sci Bull (Beijing). 2021; 66(9):925–936. https://doi.org/10.1016/j.scib.2020.12.005 PMID: 33318880

58. McCray PB Jr, Pewe L, Wohlford-Lenane C, Hickey M, Manzel L, Shi L, et al. Lethal infection of K18-hACE2 mice infected with severe acute respiratory syndrome coronavirus. J Virol. 2007; 81(2):813–821. https://doi.org/10.1128/JVI.02012-06 PMID: 17079315

59. Lian X, Hsiao C, Wilson G, Zhu K, Hazeltine LB, Azarin SM, et al. Robust cardiomyocyte differentiation from human pluripotent stem cells via temporal modulation of canonical Wnt signaling. Proc Natl Acad Sci U S A. 2012; 109(27):E1848–E1857. https://doi.org/10.1073/pnas.1200250109 PMID: 22645348

60. Sharma A, Li G, Rajarajan K, Hamaguchi R, Burridge PW, Wu SM. Derivation of highly purified cardiomyocytes from human induced pluripotent stem cells using small molecule-modulated differentiation and subsequent glucose starvation. J Vis Exp. 2015;97. https://doi.org/10.3791/52628 PMID: 25867738

61. Gauger PC, Vincent AL. Serum virus neutralization assay for detection and quantitation of serum-neutralizing antibodies to influenza A virus in swine. Methods Mol Biol. 2014; 1161:313–324. https://doi.org/10.1007/978-1-4939-0758-8_26 PMID: 24899440

62. Love MI, Huber W, Anders S. Moderated estimation of fold change and dispersion for RNA-seq data with DESeq2. Genome Biol. 2014; 15(12):550. https://doi.org/10.1186/s13059-014-0550-8 PMID: 25516281

63. Khomtchouk BB, Hennessy JR, Wahlestedt C. shinyheatmap: Ultra fast low memory heatmap web interface for big data genomics. PLoS ONE. 2017; 12(5):e0176334. https://doi.org/10.1371/journal.pone.0176334 PMID: 28493881

64. Kanehisa M, Furumichi M, Tanabe M, Sato Y, Morishima K. KEGG: new perspectives on genomes, pathways, diseases and drugs. Nucleic Acids Res. 2016; 45(D1):D353–D361. https://doi.org/10.1093/nar/gkw1092 PMID: 27899662